Submitted to ATVB

Evolving Mural Defects, Dilatation, and Biomechanical Dysfunction in Angiotensin II-Induced Thoracic Aortopathies

Dar Weiss[1], Aaron S. Long[1], George Tellides[2,3], Stéphane Avril[4], Jay D. Humphrey[1,3,*], Matthew R. Bersi[1,5]

[1]Department of Biomedical Engineering
Yale University, New Haven, CT, USA

[2]Department of Surgery and [3]Vascular Biology and Therapeutics Program
Yale School of Medicine, New Haven, CT, USA

[4]Mines Saint-Etienne, University of Lyon, University Jean Monnet, INSERM, Saint-Etienne, France

[5]Department of Mechanical Engineering and Materials Science
Washington University in St. Louis, St. Louis, MO, USA

Running Title: Evolving Thoracic Aortopathy

[*]Corresponding Author:

J.D. Humphrey, Ph.D.
Department of Biomedical Engineering
Yale University, New Haven, CT 06520 USA
jay.humphrey@yale.edu
+1-203-432-6528

Subject Terms: xxxxxxxxxxxxx

Word Count: Abstract (213), Paper minus references (6788)

Figures and Tables: 8 and 0

TOC Category – basic science

TOC Sub-Category – aneurysms (vascular biology)

Abstract

Objective – To quantify the natural history of thoracic aortopathy in a common mouse model and to identify robust correlations between measures of wall remodeling such as aortic dilatation or localized mural defects and evolving wall microstructural composition and biomechanical properties.

Approach and Results – We combined a high-resolution multi-modality imaging approach (panoramic digital image correlation and optical coherence tomography) with histopathologic examinations and biaxial mechanical testing to spatially correlate, for the first time, macroscopic mural defects and medial degeneration of the ascending aorta with local changes in aortic wall composition and mechanical properties. Results revealed strong correlations between local decreases in elastic energy storage and increases in circumferential material stiffness with increasing proximal aortic diameter and especially mural defect size. Mural defects tend to exhibit a pronounced biomechanical dysfunction that is driven by an altered organization of collagen and elastic fibers.

Conclusions – While aneurysmal dilatation is often observed within particular segments of the aorta, dissection and rupture initiate as highly localized mechanical failures. We show that wall composition and material properties are compromised in regions of local mural defects, which further increases the dilatation and overall structural vulnerability of the wall. Identification of therapies focused on promoting robust collagen accumulation may protect the wall from these vulnerabilities and limit the incidence of dissection and rupture.

Key Words: medial degeneration, dissection, wall stiffness, aortopathy, angiotensin

Introduction

Thoracic aortic aneurysms progressing to dissection (TAADs) are responsible for significant morbidity and mortality[1]. While a complex collection of cellular, molecular, and genetic factors render the aorta susceptible to TAAD[2], it is ultimately biomechanical factors such as blood pressure, wall stress, and wall strength that dictate local material and structural failures of the aortic wall. Thus, there is pressing need to understand better the evolving vulnerability of the aortic wall and the biomechanical mechanisms that promote aortic dissection and rupture[3–5]. The importance of understanding structure-function relationships of the central vasculature is underscored further by observations that uncontrolled hypertension and exuberant exercise – two incidences of excessive biomechanical loading on the aortic wall – are critical risk factors for TAAD initiation[6,7]. This is likely due to increased wall stresses exacerbating the effects of underlying mural defects rather than initiating the pathologic disease processes[8].

The ongoing discovery of genetic mutations and variants that predispose the aorta to lesion formation has led to the development of multiple models for TAAD in mice. Studies in these models have revealed critical insights into the underlying molecular mechanisms, cell pathobiology, and tissue-level changes in microstructure associated with TAAD[9–12]. Indeed, mouse models not only provide a convenient approach for studying the effects of specific genetic mutations or pharmacological interventions on vascular biology, structure, and mechanical properties, they also enable the longitudinal studies that are necessary for understanding better the natural history of conditions such as TAAD.

Chronic infusion of angiotensin II (AngII) has proven to be a useful model for studying the development of thoracic aortic lesions in mice that are characterized by local intimomedial tears, aortic dilatation, and adventitial fibrosis[13–16]. To date, however, most attention has focused on the effector cells, histological changes within the wall, or in vivo imaging of such thoracic lesions[17–20]. Although blood pressure-induced cyclic wall strains and distensibility – bulk measures of structural stiffness – have been reported to decrease with aortic dilatation[21], there remains a need for complementary studies of the associated changes in wall properties locally, particularly given that acute dissection and rupture are inherently mechanical failures. Due to the geometric complexity of AngII-induced lesions, advanced imaging and quantification methods are needed to delineate the observed intramural and regional variations in remodeling[22].

In this paper, we combine ex vivo a custom panoramic digital image correlation (pDIC) approach with optical coherence tomography (OCT) imaging and biaxial biomechanical testing to identify evolving local microstructural composition, mural degeneration, and mechanical properties of the ascending aorta as a function of the duration of AngII infusion. Despite using a standard genetically inbred hyperlipidemic

mouse strain – apolipoprotein-E-deficient (*Apoe*$^{-/-}$) on a C57BL/6J background – we found that the extent of mural defects and the degree of aortic dilatation varied considerably from mouse to mouse, consistent with prior studies focused on remodeling over a set duration of AngII infusion[16,23,24]. We thus re-classified and further analyzed the data independent from AngII duration and instead focused on either the degree of aortic dilatation or the spatial localization of mural defects, both of which revealed stronger correlations between histo-mechanical changes and thoracic aortopathy. We also found that evaluation of the type and size of the mural defect may be distorted by standard histological examinations, thus pointing to the need for higher resolution non-destructive methods – such as pDIC analysis and OCT imaging. The proposed analysis framework provides full-field information on intact geometrically-complex specimens under controlled physiologic conditions rather than relying on information solely from in vivo ultrasound which lacks information on the current mechanical state of the tissue[19] or histological sectioning which requires destructive tissue processing[16]. We submit that the present findings of highly localized evolving changes in mural defects and mechanical properties complement many prior studies on the histology and cell pathobiology of thoracic aortic lesion formation, thereby providing increased insight into the progressive deterioration of the aortic wall in this mouse model of thoracic aortopathy.

Nonstandard Abbreviations and Acronyms

AngII – angiotensin II

ANOVA – analysis of variance

Apoe$^{-/-}$ – apolipoprotein-e null mouse

pDIC – panoramic digital image correlation

OCT – optical coherence tomography

TAADs – thoracic aortic aneurysms and dissections

TGF-β – transforming growth factor-beta

Materials and Methods

All data that support the findings of this study will be made available by the corresponding author upon reasonable request. Detailed information regarding experimental data collection, mathematical modeling, and inverse material property estimation is available in the online-only Data Supplement. A description of the statistical methods used in the current study is below.

Statistical Methods. All data were first tested for normality (Kolmogorov-Smirnov test) to determine the most appropriate statistical tests. In the event that data were not normally distributed, we

used either the non-parametric Mann-Whitney U test (between two groups) or the non-parametric Kruskal Wallis one-way ANOVA on Ranks followed by Dunn's post-hoc test for multiple comparisons (between more than two groups) to compare results across study groups. When non-parametric statistics were not required, groups were compared using either Student's t-test (two groups) or one-way ANOVA with post-hoc Tukey's HSD test for multiple comparisons (more than two groups). Correlations between the various mechanical metrics and histological area fractions were assessed using the non-parametric Spearman's rank correlation coefficient, r. For all reported comparisons, a value of $p < 0.05$ was considered significant. Significant differences between or among groups are indicated in each figure.

Results

The aortic wall rapidly thickens and loses mechanical functionality with AngII infusion. One of the primary mechanical functions of the aortic wall is to store elastic energy during systolic distension and to use this energy to work on the blood during diastolic recoil to augment antegrade and retrograde blood flow[25]. In addition to its direct effects on the vessel wall, chronic infusion of AngII raises central blood pressure thus resulting in an initial increase in aortic wall stress that is often mitigated by a mechano-mediated thickening of the wall[16]. Such thickening can yet compromise mechanical function[26]. Whereas wall thickness increased quickly in the ascending aorta in response to increases in blood pressure over the first 14 days of AngII infusion, the capacity of the wall to store elastic energy diminished rapidly, suggesting the development of marked mechanical dysfunction within the first 7 days of AngII infusion (**Figure S1**). Circumferential material stiffness has also proven to be a particularly important biomechanical metric in the natural history of TAADs[21]. In contrast to the evolving changes in wall thickness and energy storage, circumferential stiffness mirrored the progressive reduction in circumferential stretch and appeared to increase slowly over 28 days of AngII infusion; axial material stiffness, on the other hand, did not change appreciably (**Figure S1**). Although local estimations of geometric and mechanical metrics varied from mouse-to-mouse, clear trends of mechanical dysfunction emerged over the time course of AngII-induced disease progression.

Evolution of mechanical properties correlates better with aortic dilatation than infusion time. Due to the geometric variations that were observed during AngII infusion, from 0 to 28 days, we next ordered the locally identified geometric and mechanical metrics as a function of the degree of mean proximal aortic dilatation, independent of the duration of AngII infusion. An unsupervised k-means clustering algorithm suggested a natural separation of the 17 overall specimens into three Groups (**Figure 1A-B, S2**): no dilatation controls (Group 1, n=3), modest AngII-induced dilatation (Group 2, n=7), and

marked AngII-induced dilatation (Group 3, *n*=7). Importantly, some of the most dilated specimens had been harvested at 14 days of infusion while many of the modestly dilated vessels had been harvested at 21 or 28 days. When data were re-classified and viewed in this way (**Figure S3**), the trends of increasing wall thickness and decreasing energy storage were similar to that of the duration of infusion. By contrast, circumferential material stiffness exhibited a more progressive increase from baseline (Group 1) through moderate-to-marked dilatation (Group 2 and 3). This k-means grouping also revealed significant negative correlations between energy storage and wall thickness that diminished with increasing aortic dilatation as well as a trend toward increasing circumferential stiffness with wall thickening. There was also a preservation of the well-known linear relationship between stiffness and wall stress across Groups 1, 2 and 3 (**Figure S4**).

Although a k-means grouping facilitates standard statistical comparisons (e.g., ANOVA), such a consolidation of the data can reduce the information content available. We thus evaluated potential correlations in key geometric and mechanical metrics on a specimen-by-specimen basis as a function of mean proximal aortic diameter (**Figure 1C**). These findings revealed stronger correlations for increasing wall thickness, decreasing stored energy, decreasing biaxial stress, and increasing circumferential stiffness with little change in axial stiffness, all with respect to increased mean aortic diameter. Recall that the duration of AngII exposure did not associate directly with dilatation (**Figure 1A, S2**). Finally, the data revealed negative correlations between measures of aortopathy and principal wall stretches (in the circumferential and axial directions) when calculated at the in vivo value of axial stretch and a distending pressure of 80 mmHg (**Figure S5**). Together, these findings support the existence of a progressive increase in structural stiffness in this model of thoracic aortopathy that has been reported previously in vivo using ultrasound[15,27].

Mural defects present regionally, but three-dimensionally. Notwithstanding the importance of overall (bulk) mechanical properties on hemodynamics, it is local material or structural vulnerabilities that give rise to dissection and rupture. OCT revealed two distinct types of localized mural defects in the ascending aorta due to AngII infusion: microscopic intramural delaminations (red asterisks; **Figure 2A**) and macroscopic partial (inner) medial ruptures (white asterisks; **Figure 2B**). Note, therefore, that none of the mice considered herein presented with a full transmural rupture of the thoracic aorta leading to extravasation of blood into the thoracic cavity. Importantly, the two types of defects often extended partially around the circumference and along the axial length of the ascending aorta, thus representing three-dimensional defects. Following individual defects along a vessel (see **Figures S6** and **Figure S7**) suggested that intramural delaminations may precede the formation of partial inner medial ruptures.

From a biomechanical perspective, it is plausible that intramural delaminations increase the wall stress locally within the intact inner portion of the wall. Such increases in stress could cause the tissue to fail mechanically and thus give rise to a partial inner medial rupture, sometimes in layers[28,29]. That the inner portion of the wall was under high mechanical stress and still highly elastic was further suggested by the marked separation of the two ends of each medial sub-layer that retracted when the layer failed (white asterisks; **Figure 2B**). The full-field OCT measurements revealed further that these mural defects tended to present predominantly in the proximal half of the ascending aorta closer to the aortic root (**Figure 3A,C** and **Figure 4A,B**). There was also a greater overall defect area found in dorsal and ventral aspects compared to lateral (inner and outer curvature) aspects of the wall (**Figure 3A,B** and **Figure 4A,B**). Though not statistically increased, outer curvature defects tended to be more prevalent than inner curvature defects across all samples (**Figure 3B**). Again, the highly localized nature of the mural defects is both clear and important.

Mural defects dictate localized changes in mechanical properties. Although total defect area appeared to increase with duration of AngII infusion, there was a strong positive correlation with the extent of dilatation, as defined by Groups 1 through 3 from unsupervised k-means clustering (dashed circles; **Figure 4C**). Moreover, overall local wall thickness (intimal-to-adventitial distance independent of intramural delamination) increased while circumferential wall stretch decreased with increasing defect area; axial wall stretch remained nearly the same independent of total defect area. Elastic energy storage and biaxial wall stress correlated negatively with defect area while circumferential stiffness correlated strongly and positively with defect area; similar to axial stretch, the axial stiffness did not vary appreciably with defect area (**Figure 4D**). As defect area related well to the degree of aortic dilatation, similar overall trends emerged when plotting the various metrics versus diameter alone (see **Figure 1C**).

To better assess the impact of three-dimensional mural defects on ascending aortic biomechanics, coupled OCT and pDIC analyses were necessary to co-localize defects and local mechanical properties. Following data acquisition and co-registration, an inverse method based on the principal of virtual power identified local material parameters for a constitutive model that has proven useful in biomechanically describing diverse blood vessels (see **Supplemental Methods** and previously published work for a detailed description of the analysis pipeline[30–34]). Using this approach, we separated the local mechanical properties – such as thickness, stored energy, and biaxial stiffness, among others – over the surface of each specimen based on their co-localization with mural defects; patches with defects are shown in red and patches without defects are shown in blue (**Figure 5A, S8, S9**). This separation was performed for all specimens with detectable defects (Group 2 and Group 3) and results were compared between individual

samples as well as across all samples in Groups 1, 2, and 3. Overall, we observed similar trends in energy storage and circumferential stiffness such that regions with mural defects tended to have lower energy storage and higher circumferential stiffness than their non-defect counterparts (**Figure 5B, S8**). Note that defect regions had a larger thickness than non-defect regions in Group 2 but a smaller thickness than non-defect regions in Group 3 (**Figure S8**). As our OCT thickness measurements include contributions from intramural delaminations (wherein thickness will appear greater due to included accumulations of amorphous material, including fluid), this provides further evidence for the natural progression of mural defects from microscopic intramural delaminations to macroscopic partial medial tears. These trends were generally true when comparing within each sample, but was more evident when comparing across groups, hence emphasizing that biomechanical dysfunction was greater in regions of mural defect.

Histo-mechanical changes correlate better with dilatation and defects than duration of infusion. It is axiomatic that local mechanical properties depend directly upon the composition and organization of the underlying material, noting that the media consists primarily of smooth muscle and elastic fibers whereas the adventitia consists primarily of fibrillar collagen. Using quantitative histological analyses, we computed medial and adventitial area for each sample (**Figure 6A**) and found that the media:adventitia ratio tended to decrease over the first 14 days of AngII infusion, but remained nearly constant thereafter to 28 days (**Figure 6C**). By contrast, when assessed based on k-means clustering Groups (**Figure 6B**), the media:adventitia ratio instead decreased as a function of aortic dilatation (**Figure 6D**). Taken together, such changes are consistent with adventitial fibrosis combined with medial damage and degeneration during AngII infusion (denoted by asterisks and arrows in histological images; **Figure 6**). As expected, these layer-specific changes were paralleled by changes in the two primary structural proteins in the wall: elastic fibers and fibrillar collagen (**Figure 6E**). Note the progressive decrease in percent elastin and increase in percent collagen, particularly in medial collagen, with increasing dilatation (**Figure 6F**). Detailed analysis of regions with mural defects (**Figure S10A**) further revealed a similar trend toward increased collagen and decreased elastin in defect regions, as compared to non-defect regions (**Figure 6G,J**); despite similar collagen content overall, birefringence analysis showed a higher percentage of thick orange fibers and a lower percentage of thin green fibers in defect regions (**Figure S10B**), suggesting a potential for collagen reinforcement following defect formation. Accumulation of other structural components, such as glycosaminoglycans (GAGs) and fibrin, was much less than that of collagen; cellular density was also minimally affected by AngII infusion (**Figure 6H,I**).

Co-registration of histo-mechanical properties reveals local structure-function relationships. Following characterization of mural defect composition, the highly localized nature and biomechanical

consequence of the mural defects demanded finer assessments, here achieved by co-registering histological (composition), OCT (wall thickness and defect location and type), and pDIC (mechanical properties) data (**Figure 7**). Importantly, whereas the pDIC and OCT data were co-registered easily given their common in vivo loading conditions, the histological sections had been fixed and processed in an unloaded configuration and in some instances distorted by the sectioning procedure. Indeed, direct comparison of OCT and histological images suggested that intramural delaminations seen on OCT often appeared as partial medial ruptures on histological examination (solid red circle; **Figure 7**), likely due to sectioning-related tearing of the highly vulnerable region around a delamination. While partial inner media tears (dashed red circles; **Figure 7**) were more conserved between OCT and histology images, there were yet several instances of distortion (i.e., larger defects) in histological images.

Co-localization of mural defects with key biomechanical metrics (white rectangles; **Figure 7**) allows direct association with local microstructural composition obtained from histology. In this regard (schematic; **Figure 8A**), it proved useful to return to the k-means groupings in seeking correlations between local composition and mechanical metrics (**Figure S11**). Indeed, the clearest histo-mechanical correlations emerged for Group 3 – the markedly dilated vessels (**Figure 8B**). Independent of defect location, collagen content correlated positively with adventitial percentage, as reported previously[31]. Whereas one expects elastically stored energy to increase with elastin content and biaxial wall stiffness to increase with collagen content, these expectations held only in regions without defects (blue curves). That is, in regions of mural defects (red curves), with low elastin and high collagen content, changes in energy storage neither increased with elastin nor decreased with collagen. Moreover, in these same regions of mural defects, the circumferential stiffness and axial stiffness tended to decrease with increasing collagen content; similar to earlier findings, axial stiffness was independent of collagen content in non-defect regions (**Figure 8B**). Taken together, these findings suggest that the histologically identified elastin and collagen are likely compromised in some cases due to either fragmentation or altered organization. Indeed, the counterintuitive reduction in stiffness with increasing collagen content suggests that thoracic aortopathy leads to changes in collagen structure or deposition (see **Figure S10B**) which potentiate the development of biomechanical dysfunction.

Discussion

Ten years after the initial observation that a chronic high-rate infusion of AngII (1000 ng/kg/min) can produce dramatic suprarenal abdominal aortic lesions in *Apoe*$^{-/-}$ mice[35], ascending aortic aneurysms were reported in the same mouse model, though with a very different pathology[13]. About the same time, it was also shown that systemic neutralization of transforming growth factor-beta (TGF-β) activity exacerbated thoracic aortic disease in AngII-infused wild-type mice[36]. Although precise roles for the renin-angiotensin system and TGF-β remain unclear in the context of TAADs[37–39], chronic AngII-infusion remains a convenient and reproducible model for studying potential mechanisms and time-courses of particular thoracic aortopathies[22] even though direct translation to human pathology is limited. Indeed, lesions typically arise rapidly in the same anatomical location, within 3-5 days of AngII infusion, and independent of hypercholesterolemia[40]. This model has also revealed initially unexpected roles of endothelial cells and fibroblasts in the evolving thoracic pathology[17,41], which is otherwise characterized by marked medial deterioration. Importantly, fragmentation of elastin and either partial or full breaks of the elastic lamellae often occur in the outer portion of the media and within the region of the outer curvature[15,40], hence emphasizing a need to study effects regionally. Finally, based on in vivo measurements of cyclic strains, it has been noted that the aortic wall becomes structurally stiffer within 3 days of AngII infusion, which persists over the typical 28 days of infusion[18,40]. Although inferences of structural stiffness do not yield information on local material properties, it appears nonetheless that increased circumferential material stiffness is a general characteristic of thoracic aortic aneurysms[16,21], which in some cases reflects an underlying dysfunctional mechanosensing or mechanoregulation of matrix[8,42]. We previously used standard biaxial testing to quantify altered bulk biaxial mechanical properties in the ascending aorta of AngII-infused *Apoe*$^{-/-}$ mice[16]. We confirmed that distensibility drops dramatically within 4 days while both wall thickness and circumferential stiffness increase progressively over the first 14 days. The increase in wall thickness paralleled the increase in blood pressure and included a marked accumulation of fibrillar collagen in the adventitia by 14 days, with a dramatic decrease in energy storage at 14 days. Although these bulk findings provide insights into the evolving mechanics, we were not able to co-localize or correlate these changes with mural defects or histological changes.

Herein, we sought to complement prior studies by correlating for the first time the evolving mural defects and local mechanical properties of the thoracic aorta in adult male *Apoe*$^{-/-}$ mice on a normal diet as a function of the duration of high-rate AngII infusion for up to 28 days. As the focus of the current study was on local biomechanical analyses of established mural defects, not biological mechanisms underlying formation and susceptibility of such defects, we only studied male mice. This choice was motivated

primarily by consistency with prior studies and the greater propensity to thoracic aortopathy in male than female *Apoe*$^{-/-}$ mice[15,16,35,40]. Toward this end, we employed a novel ex vivo multi-modality imaging approach[30–32]: pDIC provided information on surface deformations that resulted from well-controlled applied loads over a physiologic range while OCT provided critical information on through-the-wall changes in thickness and intramural structure. Together, these two high-resolution imaging methods (each on the order of 7 microns) allowed us to use a validated inverse method to quantify locally the material-specific strain energy function[30], from which one can calculate the biaxial wall stress and material stiffness that result from the underlying nonlinear, anisotropic material[43,44] (see **Supplemental Methods** for additional details). Importantly, we found that key biomechanical metrics correlated better with both the degree of mean proximal aortic dilatation and the extent of local mural defects than they did with duration of AngII infusion. Of particular note, the capacity of the ascending aorta to store energy elastically decreased with both dilatation and mural defect area while circumferential material stiffness increased with both. There was also a positive correlation between defect area and aortic diameter, suggesting that medial degeneration evidenced by partial medial tears may contribute to the observed increase in diameter[15]. Recalling that energy storage reflects a key functionality of the aorta while circumferential stiffness associates with aortic aneurysm[19], we submit that these two key metrics provide particular insight into the local biomechanics and mechanobiology of remodeling and mechanical dysfunction associated with thoracic aortopathy.

Of course, in any soft tissue, biomechanical changes result from underlying changes in microstructural composition and organization. Although they were not able to measure mechanical properties locally, a previous study using high-resolution synchrotron-based imaging reported that[15]: (i) intramural micro-hemorrhage in the ascending aorta occurred early (within 3 days of AngII infusion) and tended to occur more frequently in the outer media, (ii) elastic lamellar defects tended to emerge relatively late (18 days after initiating AngII infusion) and appeared to compromise mainly the middle lamellar structures, and (iii) dissections (defined as intramural “gaps” of at least 10% of the local wall thickness, typically with loss of continuity of at least 3 elastic lamellae) presented preferentially on the outer, not inner, curvature. Our OCT data similarly revealed more lesions on the outer curvature than inner curvature, though with a preferential dorsal / ventral rather than lateral presentation and a clear proximal (toward the aortic root) predilection. OCT also revealed microscopic intramural delaminations primarily within the inner half of the wall, which appeared to precede formation of macroscopic inner medial ruptures that reduced the effective wall thickness locally. This local thinning likely contributes to

increasing mean wall stress on the remaining portion of the intact wall surrounding the defect and may promote further damage and propagation of the defect[28].

Standard histological analysis has been the primary method for assessing wall integrity in this AngII infusion model. Our histological findings were consistent, overall, with those reported previously[15,40], but our study had the added benefit of co-localization with local material properties given our multi-modality experimental approach. Comparison of OCT and histological findings suggested that preparation of histological slides (e.g., dehydration, embedding, sectioning, and staining) may exaggerate the number and degree of inner medial ruptures. That is, additional damage likely occurs within vulnerable regions during sectioning with a microtome. We note, however, that the OCT measurements were recorded in only one (the reference state defined at 80 mmHg distending pressure and specimen-specific in vivo axial stretch) of the 42 mechanically loaded states included during pDIC testing (14 pressure states from 10 to 140 mmHg each at 3 different axial stretches ranging from the in vivo axial stretch to ±5% of the in vivo axial stretch), hence it is possible that further microscopic damage occurred during mechanical testing[45]. Nevertheless, the OCT imaging revealed complex axial variations in contiguous mural defects that typically progressed from intramural delaminations located proximally and distally to the related partial medial ruptures. Again, this suggests that the intramural delaminations may nucleate partial medial ruptures by exposing thin portions of the inner media to higher wall stresses that can contribute to defect propagation under the action of persistent hemodynamic loading in vivo[46]. We submit that ex vivo OCT imaging has the potential to reveal local defects that may otherwise be difficult to visualize in vivo given its higher spatial resolution, noting too that ex vivo pressurization was performed with a physiologic saline solution as opposed to whole blood as is the case in vivo. That these isolated portions of the media were under high wall stress and yet retained some elasticity was revealed by the highly retracted appearance of the opposing ends of the failed portions of the wall while maintained under physiological loading ex vivo. Indeed, the release of elastic energy due to tearing appears to contribute to aortic dilatation associated with AngII infusion[46]. We emphasize here that the primary goal of this study was to characterize the mechanical environment surrounding macroscopic mural defects in thoracic aortopathy, thus admitting a radially-homogenized description of material properties across the remnant wall[30–32]. Future, equally important, characterization of the mechanics of microscopic mural defects (including medial delaminations) will necessarily require discrete modeling approaches[28,46], which could also aid in modeling defect propagation, which was beyond the presence scope.

Importantly, our co-localized registrations of pDIC-OCT-histology suggested further that, in response to AngII infusion, there was an increased accumulation of fibrillar collagen around defects, but

this collagen appeared to be mechanically compromised relative to collagen in regions without mural defects. Whether this defect-related collagen was partially degraded or simply not well organized when deposited must be explored in future investigations[47–49]; such cannot be assessed by standard histology alone. Indeed, we recently found misleading histological findings in another model of aortic aneurysm comprised of abdominal elastase administration plus β–aminopropionitrile exposure[33]. It is intriguing, nonetheless, that the 14 day samples often had larger diameters than 21 and 28 day samples in the current study. Combined with our histological findings, this observation may suggest that excess collagen deposition could increase structural stability within regions of mural defect and thereby reduce (or possibly even slightly reverses) the process of aortic dilatation. That is, increasing collagen deposition in regions of mural defects may help to limit aortic dilatation and possibly dissection and rupture. Again, none of the 17 mice had transmural ruptures and we did not observe any evidence of intramural thrombus (i.e., significant fibrin on Movat staining). A possible limitation of our current study is that ex vivo biomechanical testing under axial stretching and cyclic pressurization could have removed intramural blood[15], if present, hence the absence of signs of hemorrhage need not imply an initial absence of intramural blood. This critical issue needs to be addressed in future studies as well.

In conclusion, the process of aneurysmal dilatation occurs within select regions of the central vasculature whereas aortic dissection and rupture are even more localized mechanical events. There is a pressing need, therefore, to quantify and compare both the biology and the mechanics within small regions susceptible to dissection and rupture with respect to the less affected far field tissue responses. In the current study, our multi-modality pDIC-OCT imaging approach revealed for the first time that deviations of key geometric and mechanical metrics from normal values correlate well with the mean dilatation of the proximal aorta, but especially so with the area of mural defects. Whereas two primary classes of defects emerged – microscopic intramural delaminations and macroscopic partial inner medial ruptures – our findings suggest the former may be a precursor to the latter. Regardless, regions of largest mural defect appear to have poorly organized collagen fibers and compromised elastic fibers, hence resulting in mechanical properties that render that portion of the wall not only dysfunctional, but increasingly vulnerable to mechanical failures that manifest clinically as dissection and ultimately transmural rupture. Based on the current findings, late deposition or organization of collagen may be protective, thus identification of therapeutic approaches that protect or enhance the structural collagen around regions with mural defects could reduce catastrophic vascular events, such as dissections and ruptures, and thus reduce patient morbidity and mortality.

Acknowledgments

a.We thank the excellent staff within the Yale Pathology Services for technical assistance.

b.Funding. This work was supported, in part, by grants from the US National Institutes of Health (P01 HL134605, U01 HL142518, R01 HL146723, and R00 HL146951).

c.Disclosures. The authors declare no conflicts of interest, financial or otherwise.

References

1. Pape LA, Awais M, Woznicki EM, Suzuki T, Trimarchi S, Evangelista A, Myrmel T, Larsen M, Harris KM, Greason K, Di Eusanio M, Bossone E, Montgomery DG, Eagle KA, Nienaber CA, et al. Presentation, diagnosis, and outcomes of acute aortic dissection: 17-year trends from the international registry of acute aortic dissection. *Journal of the American College of Cardiology*. 2015;66(4):350–358.
2. Wu D, Shen YH, Russell L, Coselli JS, LeMaire S a. Molecular mechanisms of thoracic aortic dissection. *The Journal of surgical research*. 2013;184(2):907–24.
3. Koullias G, Modak R, Tranquilli M, Korkolis DP, Barash P, Elefteriades J a. Mechanical deterioration underlies malignant behavior of aneurysmal human ascending aorta. *The Journal of thoracic and cardiovascular surgery*. 2005;130(3):677–83.
4. El-Hamamsy I, Yacoub MH. Cellular and molecular mechanisms of thoracic aortic aneurysms. *Nature Reviews Cardiology*. 2009;6(12):771–786.
5. Sherifova S, Holzapfel GA. Biomechanics of aortic wall failure with a focus on dissection and aneurysm: A review. *Acta Biomaterialia*. 2019;99:1–17.
6. Elefteriades JA. Thoracic aortic aneurysm: reading the enemy's playbook. *Current problems in cardiology*. 2008;33(5):203–77.
7. Hiratzka LF, Bakris GL, Beckman JA, Bersin RM, Carr VF, Casey DE, Eagle KA, Hermann LK, Isselbacher EM, Kazerooni EA, Kouchoukos NT, Lytle BW, Milewicz DM, Reich DL, Sen S, et al. 2010 ACCF/AHA/AATS/ACR/ASA/SCA/SCAI/SIR/STS/SVM guidelines for the diagnosis and management of patients with thoracic aortic disease: Executive summary: A report of the american college of cardiology foundation/american heart association task force on pra. *Circulation*. 2010;121(13):266–369.
8. Latorre M, Humphrey JD. Numerical knockouts–In silico assessment of factors predisposing to thoracic aortic aneurysms. *PLoS Computational Biology*. 2020;16(10):1–25.
9. Lindsay ME, Dietz HC. The genetic basis of aortic aneurysm. *Cold Spring Harbor Perspectives in Medicine*. 2014;4(9).
10. Pinard A, Jones GT, Milewicz DM. Genetics of Thoracic and Abdominal Aortic Diseases: Aneurysms, Dissections, and Ruptures. *Circulation Research*. 2019;124(4):588–606.
11. Creamer TJ, Bramel EE, Macfarlane EG. Insights on the pathogenesis of aneurysm through the study of hereditary aortopathies. *Genes*. 2021;12(2):1–44.
12. Faggion Vinholo T, Brownstein AJ, Ziganshin BA, Zafar MA, Kuivaniemi H, Body SC, Bale AE, Elefteriades JA. Genes Associated with Thoracic Aortic Aneurysm and Dissection: 2019 Update

and Clinical Implications. *Aorta (Stamford, Conn.)*. 2019;7(4):99–107.

13. Daugherty A, Rateri DL, Charo IF, Owens AP, Howatt DA, Cassis LA. Angiotensin II infusion promotes ascending aortic aneurysms: attenuation by CCR2 deficiency in apoE-/- mice. *Clinical science (London, England : 1979)*. 2010;118(11):681–9.

14. Zhang X, Thatcher SE, Rateri DL, Bruemmer D, Charnigo R, Daugherty A, Cassis L a. Transient exposure of neonatal female mice to testosterone abrogates the sexual dimorphism of abdominal aortic aneurysms. *Circulation research*. 2012;110(11):e73-85.

15. Trachet B, Piersigilli A, Fraga-Silva RA, Aslanidou L, Sordet-Dessimoz J, Astolfo A, Stampanoni MFMM, Segers P, Stergiopulos N. Ascending Aortic Aneurysm in Angiotensin II-Infused Mice: Formation, Progression, and the Role of Focal Dissections. *Arteriosclerosis, thrombosis, and vascular biology*. 2016;36(4):673–81.

16. Bersi MR, Khosravi R, Wujciak AJ, Harrison DG, Humphrey JD. Differential cell-matrix mechanoadaptations and inflammation drive regional propensities to aortic fibrosis, aneurysm or dissection in hypertension. *Journal of the Royal Society, Interface*. 2017;14(136):1–31.

17. Rateri DL, Moorleghen JJ, Balakrishnan A, Owens AP, Howatt DA, Subramanian V, Poduri A, Charnigo R, Cassis LA, Daugherty A. Endothelial cell-specific deficiency of Ang II type 1a receptors attenuates Ang II-induced ascending aortic aneurysms in LDL receptor-/- mice. *Circulation research*. 2011;108(5):574–81.

18. Favreau JT, Nguyen BT, Gao I, Yu P, Tao M, Schneiderman J, Gaudette GR, Ozaki CK. Murine ultrasound imaging for circumferential strain analyses in the angiotensin II abdominal aortic aneurysm model. *Journal of vascular surgery*. 2012;56(2):462–9.

19. Phillips EH, Di Achille P, Bersi MR, Humphrey JD, Goergen CJ. Multi-modality imaging enables detailed hemodynamic simulations in dissecting aneurysms in mice. *IEEE Transactions on Vehicular Technology*. 2017;36(6):1297–1305.

20. He C, Jiang B, Wang M, Ren P, Murtada S, Caulk AW, Li G, Qin L, Assi R, Lovoulos CJ, Schwartz MA, Humphrey JD, Tellides G. mTOR inhibition prevents angiotensin II-induced aortic rupture and pseudoaneurysm but promotes dissection in Apoe-deficient mice. *JCI insight*. 2022;7(3).

21. Bellini C, Bersi MR, Caulk AW, Ferruzzi J, Milewicz DM, Ramirez F, Rifkin DB, Tellides G, Yanagisawa H, Humphrey JD. Comparison of 10 murine models reveals a distinct biomechanical phenotype in thoracic aortic aneurysms. *Journal of the Royal Society, Interface*. 2017;14(130):20161036.

22. Sheppard MB, Daugherty A, Lu H. Insights into ascending aortic aneurysm pathogenesis using in vivo and ex vivo imaging systems in angiotensin II-infused mice. *Journal of thoracic disease*. 2016;8(8):E822-4.

23. Trachet B, Fraga-Silva RA, Piersigilli A, Tedgui A, Sordet-Dessimoz J, Astolfo A, Van der Donckt C, Modregger P, Stampanoni MFM, Segers P, Stergiopulos N. Dissecting abdominal aortic aneurysm in Ang II-infused mice: suprarenal branch ruptures and apparent luminal dilatation. *Cardiovascular Research*. 2014;105(2):213–222.

24. Trachet B, Aslanidou L, Piersigilli A, Fraga-Silva RA, Sordet-Dessimoz J, Villanueva-Perez P, Stampanoni MFM, Stergiopulos N, Segers P. Angiotensin II infusion into ApoE-/- mice: a model for aortic dissection rather than abdominal aortic aneurysm? *Cardiovascular Research*. 2017;113(10):1230–1242.

25. Humphrey JD, Harrison DG, Figueroa CA, Lacolley P, Laurent S. Central Artery stiffness in hypertension and aging a problem with cause and consequence. *Circulation Research*. 2016;118(3):379–381.

26. Bersi MR, Bellini C, Wu J, Montaniel KRC, Harrison DG, Humphrey JD. Excessive adventitial remodeling leads to early aortic maladaptation in angiotensin-induced hypertension. *Hypertension*. 2016;67(5):890–896.

27. Sawada H, Chen JZ, Wright BC, Moorleghen JJ, Lu HS, Daugherty A. Ultrasound Imaging of the Thoracic and Abdominal Aorta in Mice to Determine Aneurysm Dimensions. *Journal of visualized experiments : JoVE*. 2019;(145).

28. Ban E, Cavinato C, Humphrey JD. Differential propensity of dissection along the aorta. *Biomechanics and Modeling in Mechanobiology*. 2021;(0123456789).

29. Roccabianca S, Bellini C, Humphrey JD. Computational modelling suggests good, bad and ugly roles of glycosaminoglycans in arterial wall mechanics and mechanobiology. *Journal of the Royal Society, Interface*. 2014;11(97):20140397.

30. Bersi MR, Bellini C, Di Achille P, Humphrey JD, Genovese K, Avril S. Novel methodology for characterizing regional variations in material properties of murine aortas. *Journal of Biomechanical Engineering*. 2016;138(July):1–15.

31. Bersi MR, Bellini C, Humphrey JD, Avril S. Local variations in material and structural properties characterize murine thoracic aortic aneurysm mechanics. *Biomechanics and modeling in mechanobiology*. 2019;18(1):203–218.

32. Weiss D, Cavinato C, Gray A, Ramachandra AB, Avril S, Humphrey JD, Latorre M. Mechanics-driven mechanobiological mechanisms of arterial tortuosity. *Science Advances*. 2020;6(49).

33. Weiss D, Latorre M, Rego B V, Cavinato C, Tanski BJ, Berman AG, Goergen CJ, Humphrey JD. Biomechanical consequences of compromised elastic fiber integrity and matrix cross-linking on abdominal aortic aneurysmal enlargement. *Acta biomaterialia*. 2021;134:422–434.

34. Genovese K, Badel P, Cavinato C, Pierrat B, Bersi MR, Avril S, Humphrey JD. Multi-view Digital Image Correlation Systems for In Vitro Testing of Arteries from Mice to Humans. *Experimental Mechanics*. 2021;(Dic).

35. Daugherty A, Manning MW, Cassis LA. Angiotensin II promotes atherosclerotic lesions and aneurysms in apolipoprotein E-deficient mice. *The Journal of clinical investigation*. 2000;105(11):1605–12.

36. Wang Y, Ait-Oufella H, Herbin O, Bonnin P, Ramkhelawon B, Taleb S, Huang J, Offenstadt G, Combadière C, Rénia L, Johnson JL, Tharaux P, Tedgui A, Mallat Z. TGF-beta activity protects against inflammatory aortic aneurysm progression and complications in angiotensin II-infused mice. *The Journal of clinical investigation*. 2010;120(2):422–32.

37. Angelov SN, Hu JH, Wei H, Airhart N, Shi M, D'Ichek DA. TGF-β (transforming growth factor-β) signaling protects the thoracic and abdominal aorta from angiotensin iiinduced pathology by distinct mechanisms. *Arteriosclerosis, Thrombosis, and Vascular Biology*. 2017;37(11):2102–2113.

38. Tellides G. Further evidence supporting a protective role of transforming growth factor-β (TGFβ) in aortic aneurysm and dissection. *Arteriosclerosis, Thrombosis, and Vascular Biology*. 2017;37(11):1983–1986.

39. van Dorst DCH, de Wagenaar NP, van der Pluijm I, Roos-Hesselink JW, Essers J, Danser AHJ.

Transforming Growth Factor-β and the Renin-Angiotensin System in Syndromic Thoracic Aortic Aneurysms: Implications for Treatment. *Cardiovascular Drugs and Therapy*. 2021;35(6):1233–1252.

40. Rateri DL, Davis FM, Balakrishnan A, Howatt D a, Moorleghen JJ, O'Connor WN, Charnigo R, Cassis L a, Daugherty A. Angiotensin II induces region-specific medial disruption during evolution of ascending aortic aneurysms. *The American journal of pathology*. 2014;184(9):2586–95.

41. Poduri A, Rateri DL, Howatt D a., Balakrishnan A, Moorleghen JJ, Cassis L a., Daugherty A. Fibroblast Angiotensin II type 1a receptors contribute to Angiotensin II-induced medial hyperplasia in the ascending aorta. *Arteriosclerosis, Thrombosis, and Vascular Biology*. 2015;35(9):1995–2002.

42. Humphrey JD, Schwartz M a., Tellides G, Milewicz DM. Role of mechanotransduction in vascular biology: focus on thoracic aortic aneurysms and dissections. *Circulation research*. 2015;116(8):1448–61.

43. Ferruzzi J, Bersi MR, Humphrey JD. Biomechanical phenotyping of central arteries in health and disease: advantages of and methods for murine models. *Annals of biomedical engineering*. 2013;41(7):1311–30.

44. Mousavi SJ, Farzaneh S, Avril S. Patient-specific predictions of aneurysm growth and remodeling in the ascending thoracic aorta using the homogenized constrained mixture model. *Biomechanics and Modeling in Mechanobiology*. 2019;18(6):1895–1913.

45. Ferruzzi J, Murtada SI, Li G, Jiao Y, Uman S, Ting MY, Tellides G, Humphrey JD. Pharmacologically Improved Contractility Protects Against Aortic Dissection in Mice With Disrupted Transforming Growth Factor-beta Signaling Despite Compromised Extracellular Matrix Properties. *Arteriosclerosis, Thrombosis, and Vascular Biology*. 2016;36(5):919–927.

46. Ban E, Cavinato C, Humphrey JD. Critical Pressure of Intramural Delamination in Aortic Dissection. *Annals of biomedical engineering*. 2022;50(2):183–194.

47. Iliopoulos DC, Kritharis EP, Giagini AT, Papadodima S a, Sokolis DP. Ascending thoracic aortic aneurysms are associated with compositional remodeling and vessel stiffening but not weakening in age-matched subjects. *The Journal of thoracic and cardiovascular surgery*. 2009;137(1):101–9.

48. Cavinato C, Chen M, Weiss D, Ruiz-Rodríguez MJ, Schwartz MA, Humphrey JD. Progressive Microstructural Deterioration Dictates Evolving Biomechanical Dysfunction in the Marfan Aorta. *Frontiers in Cardiovascular Medicine*. 2021;8(December):1–11.

49. Ruddy JM, Jones JA, Stroud RE, Mukherjee R, Spinale FG, Ikonomidis JS. Differential effects of mechanical and biological stimuli on matrix metalloproteinase promoter activation in the thoracic Aorta. *Circulation*. 2009;120(SUPPL. 1):262–268.

50. Bersi MR, Acosta Santamaría VA, Marback K, Di Achille P, Phillips EH, Goergen CJ, Humphrey JD, Avril S. Multimodality Imaging-Based Characterization of Regional Material Properties in a Murine Model of Aortic Dissection. *Scientific Reports*. 2020;10(1):1–23.

51. Humphrey JD. *Cardiovascular Solid Mechanics*. New York, NY: Springer New York; 2002.

52. Maas SA, Ellis BJ, Ateshian GA, Weiss JA. FEBio: finite elements for biomechanics. *Journal of biomechanical engineering*. 2012;134(1):011005.

53. Rocha KR, Yezzi AJ, Prince JL. A hybrid Eulerian-Lagrangian approach for thickness,

correspondence, and gridding of annular tissues. *IEEE Transactions on Image Processing*. 2007;16(3):636–648.

54. Yezzi AJ, Prince JL. An Eulerian PDE approach for computing tissue thickness. *IEEE transactions on medical imaging*. 2003;22(10):1332–9.

55. Humphrey JD, Tellides G. Central artery stiffness and thoracic aortopathy. *American Journal of Physiology - Heart and Circulatory Physiology*. 2019;316(1):H169–H182.

Highlights (3-5)

- Combining high-resolution methods for imaging (optical coherence tomography), biomechanical analysis (panoramic digital image correlation), and quantitative histological analysis enables determination of local structure-function relationships in murine the aorta.

- Co-localization of mural composition, defects, and mechanical properties reveals marked biomechanical dysfunction of the aneurysmal ascending aortic wall characterized by loss of energy storage capability and higher circumferential stiffness.

- Microscopic mural defects (medial delaminations) likely precede macroscopic defects (partial medial tears) due to redistributions of wall stress from damaged to initially undamaged tissue.

- Promoting robust collagen accumulation within regions of local mural degeneration and thoracic aortopathy promise to protect the wall from catastrophic mechanical failure and should be pursued.

Figures and Captions

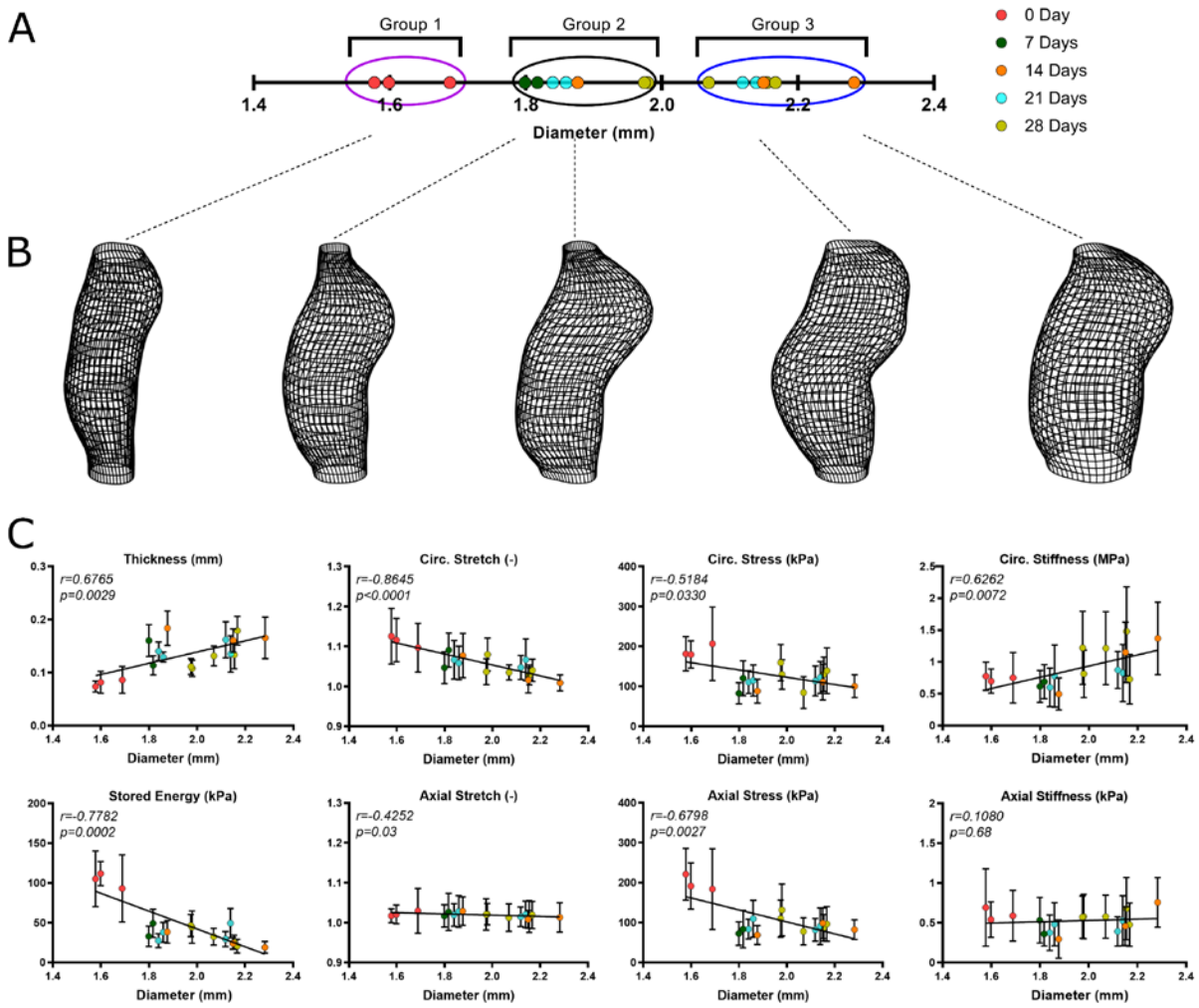

Figure 1. ***Local ascending aortic biomechanical dysfunction correlates with proximal aortic diameter.*** Analysis of key geometric and biaxial mechanical metrics as a function of proximal aortic diameter, rather than duration of AngII infusion, reveals strong correlations. (**A**) Distribution of mean proximal aortic diameters for all tested specimens (n=17 total); samples were tested after 0 days (n =3), 7 days (n=2), 14 days (n=3), 21 days (n=4), or 28 days (n=5) of AngII infusion. Unsupervised k-means clustering identified three groups based on mean diameter (magenta, black, and blue ellipses; see **Figure S2** and **Figure S3**). (**B**) Representative 3D wireframe geometry reconstructions from pDIC testing. Samples are oriented with the distal end (just past the brachiocephalic artery) at the top and the proximal end (towards the root) at the bottom; the dilatation at the top-right of each sample is the ligated aortic arch. (**C**) Correlations of eight key geometric and mechanical metrics as a function of mean proximal aortic diameter with average ± standard error data shown for all samples (circle colors indicate the duration of AngII infusion, as in **Figure 1A**). Each average data point represents up to 1000 localized assessments (40 circumferential locations × 25 axial locations) per specimen. All values are calculated at a fixed value of 100 mmHg across samples and circumferential (circ) and axial stretches are computed relative to an in vivo reference configuration defined ex vivo at 80 mmHg distending pressure and the specimen-specific value of the in

vivo axial stretch. Correlation strength was evaluated by the Spearman rank correlation coefficient *r* with correlation coefficients and *p*-values reported for each comparison.

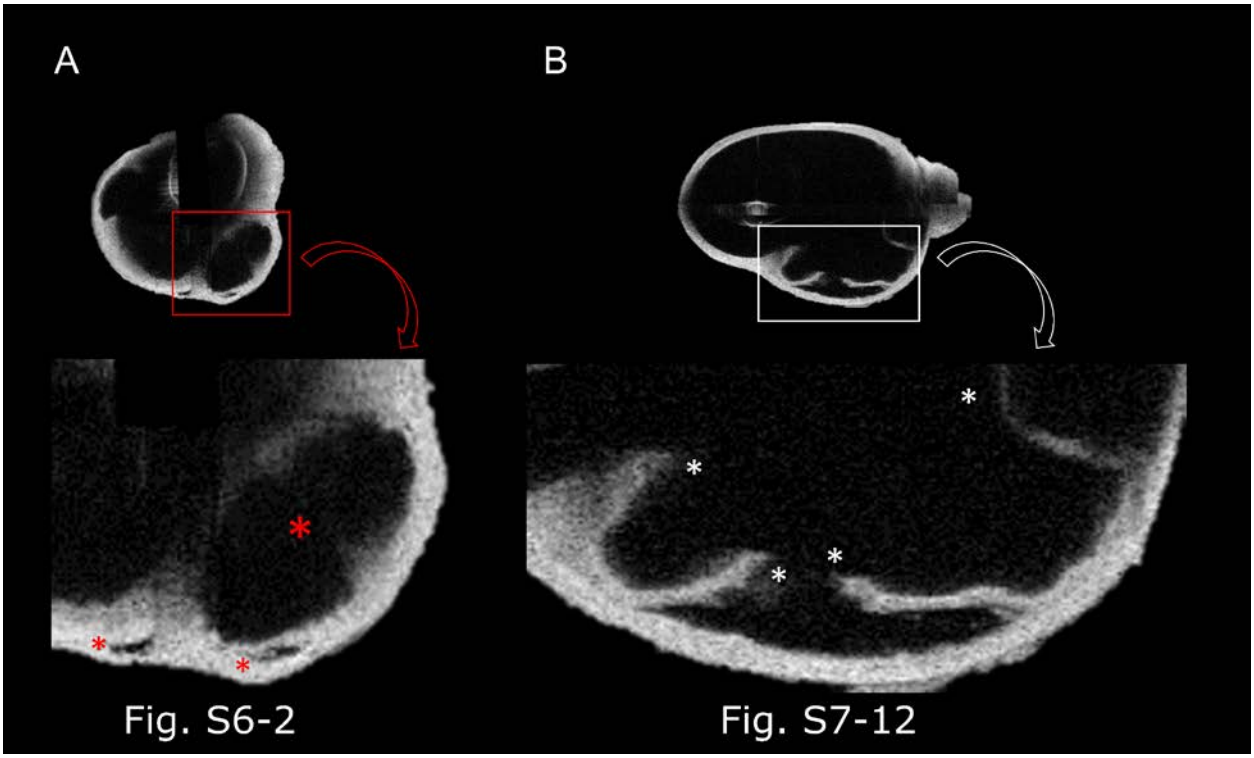

Figure 2. ***OCT imaging of thoracic aortopathy samples reveals two primary types of mural defects.*** Representative OCT images highlight the two primary types of mural defects observed – intramural delaminations and partial medial ruptures. (**A**) Intramural delaminations are indicated by apparent gaps within the vessel wall that can be small or large (red asterisks). (**B**) Partial medial ruptures can present as two distinctly torn medial aspects (white asterisks) that mimics intimal flap presentation. In both instances, defects were typically less than half of the distance from the root to the brachiocephalic artery (toward the proximal end of the specimen). The cross-sections shown are selected from the 100 OCT cross-sections available for each sample (note **Figure S6** and **Figure S7** contain ~20 successive cross-sections to visualize the 3D nature of the mural defects).

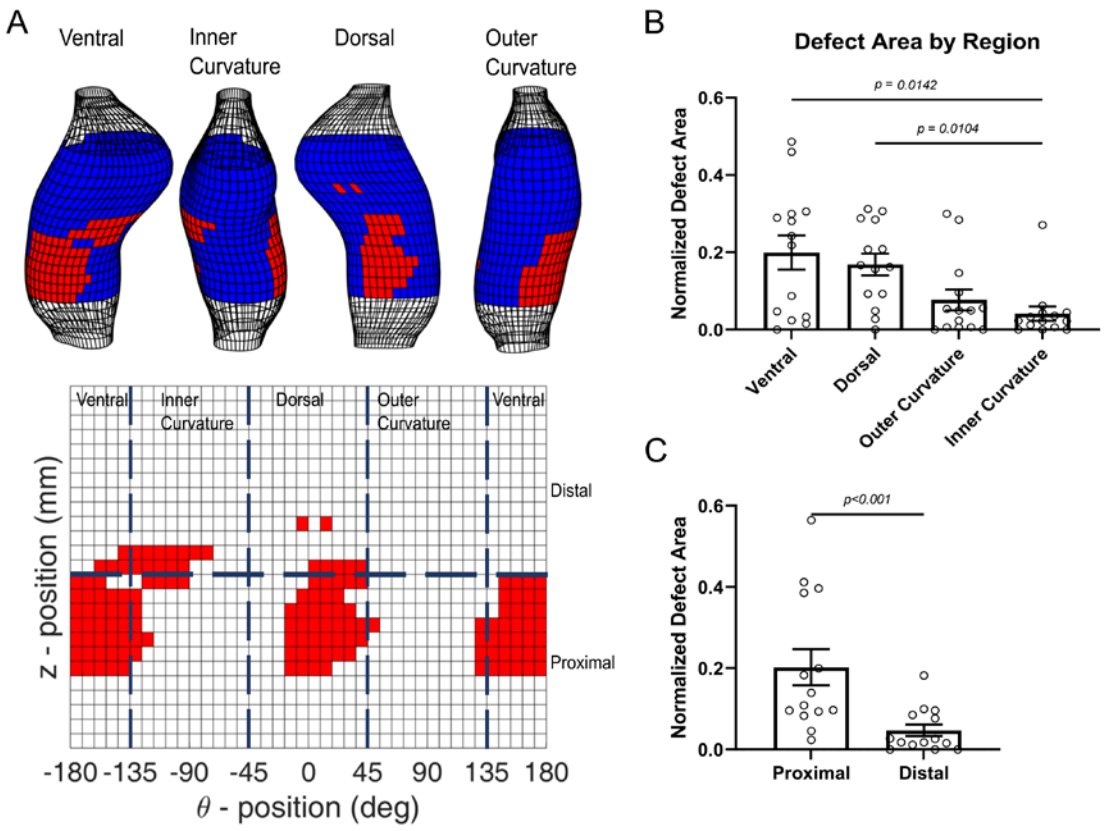

Figure 3. ***OCT imaging reliably identifies the location and size of mural defects.***
Semiautomatic analysis of OCT cross-sections revealed the spatial localization of mural defects. (**A**) Mural defect map for a representative specimen, with the regions with local defects shown in red and regions without local defects shown in blue. Defect locations have been mapped on the co-registered 3D geometry reconstructed from pDIC (top) and are also shown in a 2D representation (bottom). Note the outer curvature is aligned at 0° to allow for repeatable definitions of dorsal-ventral and inner-out curvature quadrants across specimens; proximal and distal are defined as the lower and upper half of the sample, as shown. (**B**) Analysis of all samples with measurable defects (in Group 2 and Group 3) revealed a preferential defect localization on the dorsal and ventral sides over the inner and outer curvature. (**C**) Additionally, defects were typically located in the proximal half of specimens (toward the aortic root). Non-parametric Kruskal Wallis one-way ANOVA followed by Dunn's post-hoc test for multiple comparisons (panel B) or Mann-Whitney U test (panel C).

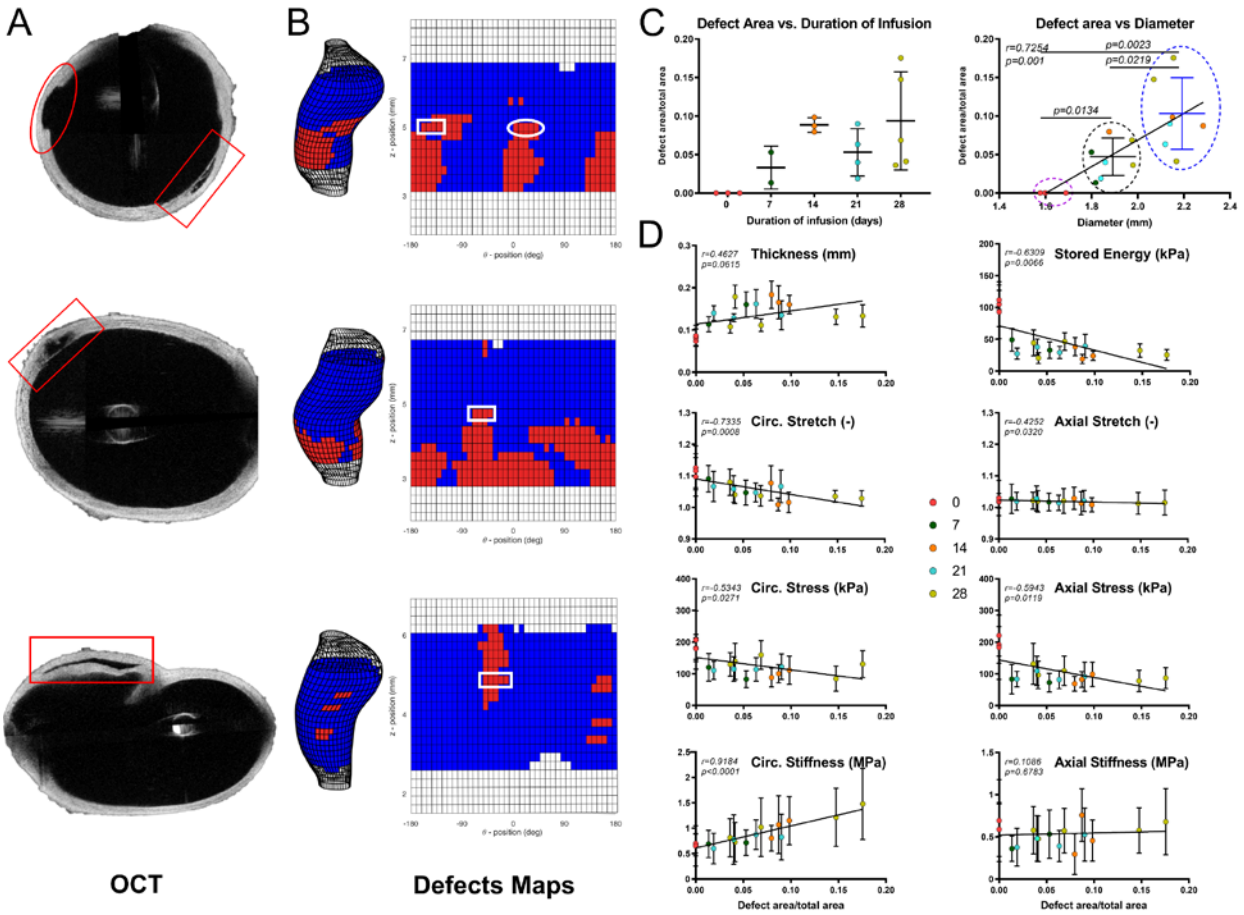

Figure 4. ***Local ascending aortic biomechanical dysfunction also correlates with mural defect size.*** (**A**) Mural defects in OCT cross-sectional images typically present as either intramural delaminations (red rectangles) or partial medial tears (red ellipse). (**B**) Regional variations in mural defects can be extracted from OCT images and projected onto 3D geometry reconstructions from pDIC or 2D defect maps. (**C**) The extent of defect area (normalized by total area in 2D maps) tended to have a weak positive correlation with duration of AngII infusion (left), but showed strong correlations with mean proximal aortic diameter (right) and k-means clustering Groups 1, 2, and 3 (dashed ellipse; right). Marker colors indicate the duration of AngII infusion. (**D**) Correlation analysis revealed strong relationships between key geometric and mechanical metrics and normalized defect area. In particular, note the decrease in stored energy and biaxial stress and the increase in thickness and circumferential stiffness with increasing normalized defect area. Correlation strength was evaluated by the Spearman rank correlation coefficient *r* with correlation coefficients and *p*-values reported for each comparison.

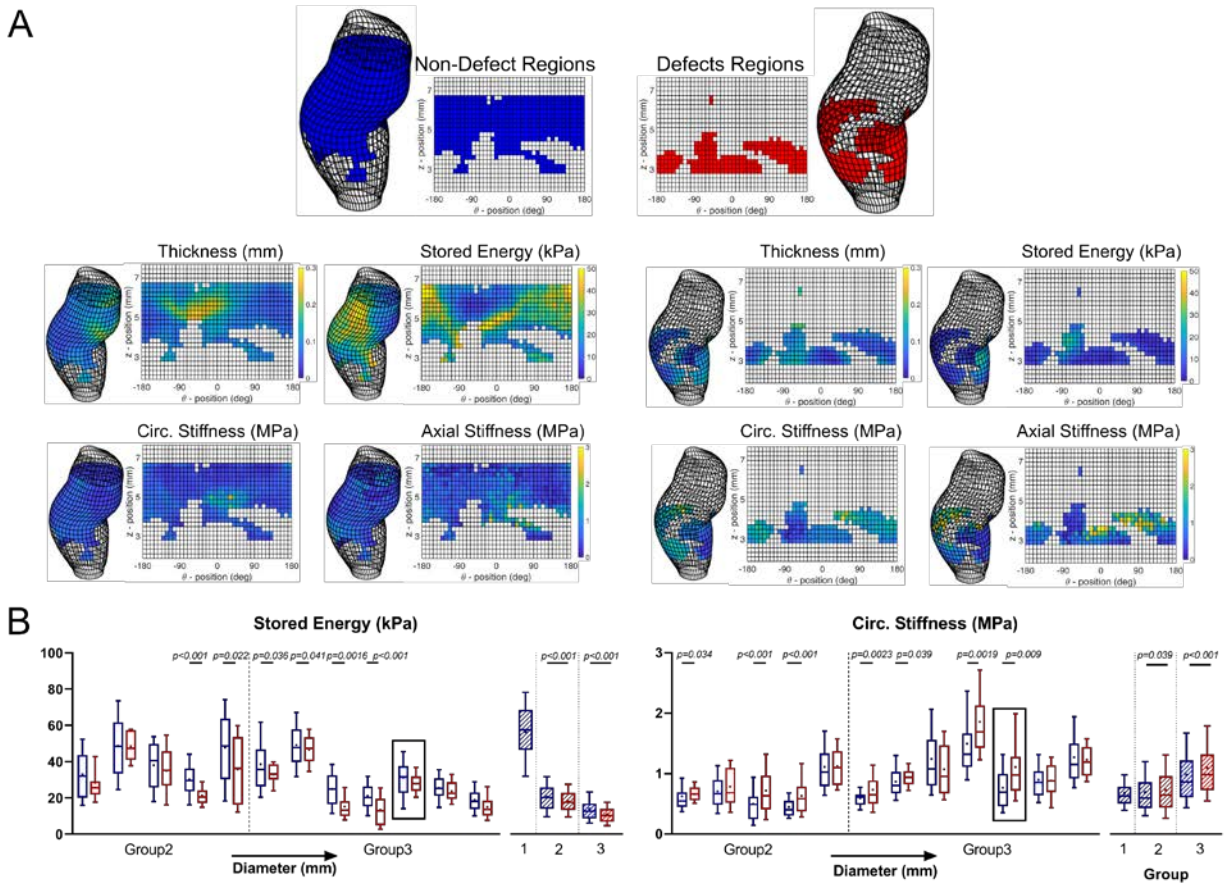

Figure 5. ***Local mural defects tend to have worse biomechanical dysfunction than non-defect regions.*** (**A**) Representative 3D ascending aortic shape reconstructions and unwrapped 2D property maps showing geometric and mechanical metrics for regions without mural defects (blue; left) or regions with underlying defects (red; right). Spatial distributions of four key metrics – wall thickness, stored energy, and circumferential and axial stiffness – are shown for defect and non-defect regions. (**B**) Locally identified distributions of stored energy and circumferential stiffness for each sample (up to 1000 data points per sample) in Group 2 and 3 ordered from left to right according to the mean proximal aortic diameter (open bars) as well as for all data points within each group (filled bars); analysis of regions with and without defects are denoted by red and blue bars, respectively. Black box corresponds to the specimen shown in the representative 3D and 2D parameter maps. Note that the decreases in elastic energy storage and increases in circumferential material stiffness are generally exacerbated in the defect regions relative to the non-defect regions (see **Figure S8** and **S9** for additional biomechanical metrics). Non-parametric Kruskal Wallis one-way ANOVA followed by Dunn's post-hoc test for multiple comparisons.

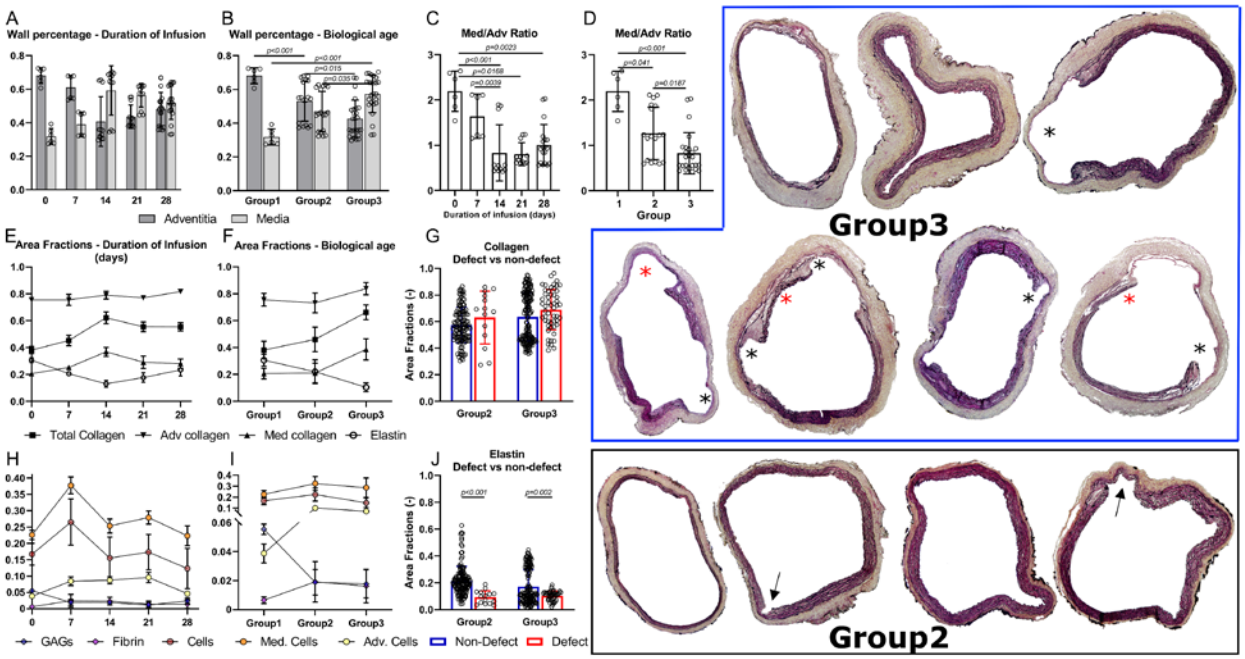

Figure 6. ***Histological analysis reveals microstructural changes associated with thoracic aortopathy.*** Quantification of Movat-stained histological images was initially focused on changes in the percentage of the wall occupied by media and adventitia (**A**) over the course of AngII infusion or (B) as a function of k-means clustering groups. (**C**) The ratio of media/adventitia tended to decrease non-monotonically over AngII whereas (**D**) the decrease was more apparent when comparing across Groups 1, 2, and 3. (**E, F**) This layer-specific change was consistent with the general percent increase in collagen and decrease in elastin, due in part to deposition of the former and fragmentation of the latter (red asterisks, right). (**H, I**) Marginal changes in GAGs, fibrin, and cellular density were observed across time points or k-means groups. Illustrative histological cross-sections from Group 2 (moderate dilatation) and Group 3 (marked dilatation) lesions contain many cases of localized partial (black arrows, right) or full medial ruptures (black asterisks, right) despite an intact adventitia. Local analysis over each histological cross-section (see **Figure S10**) revealed (**G**) a trend toward increased collagen and (**J**) decreased elastin in regions with mural defects, compared to non-defect regions. Non-parametric Kruskal Wallis one-way ANOVA followed by Dunn's post-hoc test for multiple comparisons.

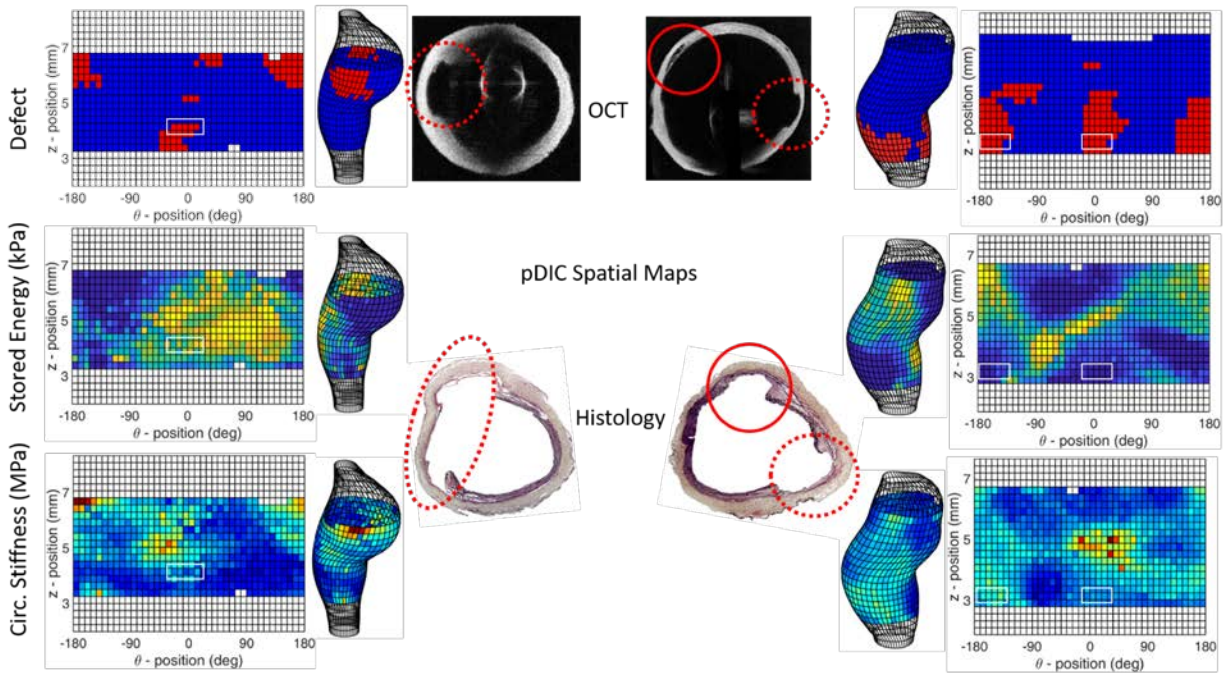

Figure 7. ***Co-registration between modalities enables comparison of local mechanical properties with underlying tissue microstructure.***

Spatial co-registration of (**top row**) OCT inferred regions of mural defects with pDIC maps of identified material properties such as stored energy and circumferential stiffness (**middle row** and **bottom row**) and histological composition (**center**) facilitates development of local structure-function relationships in thoracic aortopathy samples. This process is illustrated for two representative samples with intramural delaminations (solid red ellipse) and partial medial tears (dashed red ellipses); white rectangles indicate locations of mural defect in parameter maps. In addition to compositional and mechanical analysis of mural defects, this approach highlights that visualization of defect areas appear to be exaggerated in histological sections (defects within dashed ellipses appear larger), relative to OCT. This is likely due in part to microtome-based sectioning artifacts arising in regions of compromised structural integrity.

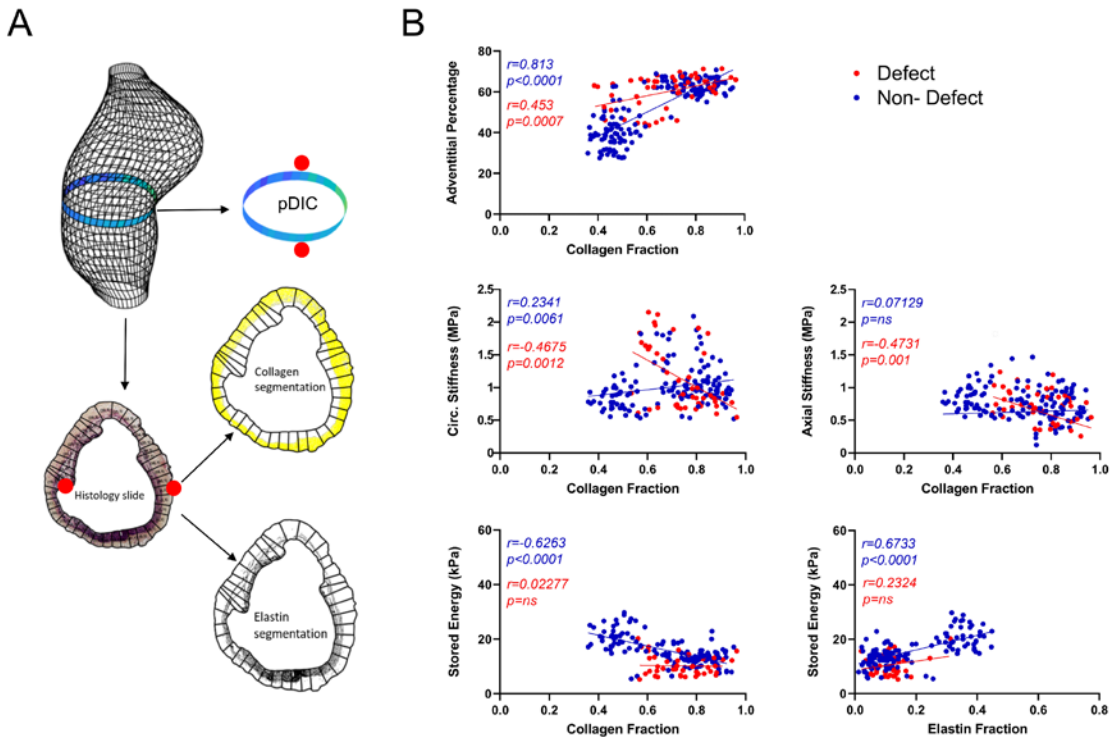

Figure 8. Histo-mechanical correlations reveal the contribution of microstructural composition to local mural defect biomechanics.

(**A**) Schematic representation of the co-registration procedure for comparing OCT, pDIC, and histological results. Note that regional histological analysis, was performed independently for 40 circumferential sectors for consistency with the number of circumferential patches in the inverse material parameter estimation. (**B**) Correlations for key geometric and mechanical metrics as a function of local elastin and collagen fraction in k-means clustering Group 3 (see **Figure S11** for Group 1 and Group 2). Note that these two structural proteins endow the wall with its energy storing capacity (i.e., resilience) and stiffness / strength (i.e., structural integrity), respectively. Correlation analysis has been performed separately for regions with mural defects (red) and regions without mural defects (blue). Defect regions tended to have lower elastin content and attenuated increases in energy storage with increasing elastin as well as reduced biaxial material stiffness with increasing collagen fraction. Both of these findings suggest the collagen and elastin remaining within defect regions are potentially compromised though they are often present histologically. Correlation strength was evaluated by the Spearman rank correlation coefficient *r* with correlation coefficients and *p*-values reported for each comparison.